

A detailed modelling of the chemically rich clumps along the CB3 outflow

Milena Benedettini^{1,2*}, Jeremy A. Yates², Serena Viti² and Claudio Codella³

¹INAF-Istituto di Fisica dello Spazio Interplanetario, Area di Ricerca di Tor Vergata, via del Fosso del Cavaliere 100, 00133 Roma, Italy

²Department of Physics and Astronomy, University College London, Gower Street, London, WC1E6BT, UK

³INAF-Istituto di Radioastronomia, Sezione di Firenze, Largo E. Fermi 5, 50125 Firenze, Italy

Accepted . Received .

ABSTRACT

In order to investigate the origin and the structure of the low velocity, chemically rich clumps observed along the lobes of low- and intermediate-mass outflows, we construct a detailed model of the S1 clump along the CB3 outflow. We use a time-dependent chemical model coupled with a radiative transfer model to reproduce the observed line profile for a direct comparison with previous observations of this clump. We find that the simultaneous fitting of multiple species and transitions is a powerful tool in constraining the physical parameters of the gas. Different scenarios for the clump formation have been investigated. The models that better reproduce all the observed lines are those where the clump is formed, at least partially, before the advent of the outflow; with the advent of the outflow the clump undergoes a short period of non-dissociative shock and the consequent release of the icy mantle together with the high temperature chemistry leads to the observed chemical enrichment. Our results also suggest the presence of substructure within the clump: a more extended component traced by CS, SO and the lower energy transitions (3_K-2_K and 2_K-1_K) of CH_3OH , and a more compact component traced by H_2CO , SO_2 and the higher energy transitions (5_K-4_K) of CH_3OH .

Key words: ISM: individual:CB3 - ISM: jets and outflows - ISM: molecules.

1 INTRODUCTION

Bipolar molecular outflows are ubiquitously present around Young Stellar Objects (YSOs) and are associated with the very early stages of star formation (e.g. Richer et al. 2000).

A large range of excitation conditions and a significant chemical differentiation are present along the lobes of the outflows. The shock-excited gas cools mainly radiatively via the emission of atomic and molecular species whose abundances are strongly enhanced by the shocks generated by the interaction between the protostellar wind and the molecular cloud. High velocity ($v \geq 100 \text{ km s}^{-1}$) clumps, the so called molecular bullets, are detected along the axis of some outflows. The prototype of such bullets are those observed in SiO in the lobes of the L1148 outflow (Bachiller et al. 1991) but they generally show weak emission of other molecular lines. A few outflows however, e.g. L1157 and CB3 (Bachiller et al. 2001, Codella & Bachiller 1999), have a particular rich emission spectrum with molecular clumps at relatively low velocity ($v \leq 10 \text{ km s}^{-1}$). These molecular clumps show emission from molecular species usually unobserved

along outflows and they have dimensions which do not exceed 0.1 pc. While the high velocities and high abundance of SiO suggest that the molecular bullets are most likely associated with mini-bow shocks formed by the outflow propagation (e.g. Deutrey et al. 1997), the origin of the low velocity clumps is not yet clear. In a recent study Viti et al. (2004) (thereafter Paper I), have investigated two possibilities for the origin of the low velocity clumps: i) the clumps are formed by episodic mass loss of the forming object or ii) the clumps are density structure pre-existing the advent of the outflow and the effect of the outflow is to accelerate and shock them, altering their chemistry. Paper I used a chemical model to simulate the clump formation and its subsequent interaction with the outflow and inferred that the low velocity outflow clumps are probably density structures formed, at least partly, prior of the advent of the outflow. With the advent of the outflow, not only the temperature of the clumps increases ($\sim 100 \text{ K}$), but the clumps also undergo a short period of non-dissociative shock. This preliminary conclusion was reached by comparing the column densities derived by the chemical models with existing single dish observations along the CB3 (Codella & Bachiller 1999) and L1157 outflows (Bachiller et al. 2001). The shortcomings of

* E-mail: milena.benedettini@ifsi-roma.inaf.it

such an analysis were that the estimations of the column densities derived from the chemical models, as well as those derived from the observations, suffer from high uncertainties due to the fact that some of the parameters required to calculate them may be unknown. In particular, to estimate the observed column densities arbitrary assumptions have to be made regarding LTE conditions, excitation temperatures and the lines being optically thin. On the other hand, the theoretical calculation of column densities from the chemical model required knowledge of the geometry of the emitting region. However, when dealing with small emitting regions, such as the low velocity clumps along molecular outflows, the observations (usually single dish with spatial resolution of few tens of arcsec) do not constrain such geometry. If more transitions of the same species are available, one can use a Large Velocity Gradient (LVG) model to derive the density and temperature of the emitting gas but even in such cases often the results have a large uncertainty because the observed line ratios are not always sensitive to the temperature or density.

One way to reduce the number of arbitrary assumptions is to model *directly* the observed line emission using a radiative transfer model that predicts the line profile, a method already adopted by other authors (e.g. Jørgesen et al. 2004, Doty et al. 2004 and Schöier et al. 2002). In this work we attempt such an approach by coupling the time dependent chemical model of Paper I with the radiative transfer model Spherical Multi-Mol (SMMOL) (Rawlings & Yates 2001). In particular, we expand the grids of chemical models computed in Paper I and use them as input parameters for the radiative transfer model to simulate the line profiles of several species and, where possible, of multiple transitions of the same species. We then simultaneously fit such profiles with the observations of CB3 and attempt to constrain the physical parameters of the emitting gas and thus their formation scenario. The paper is organized as follow: in Section 2 both the chemical and the radiative transfer models are briefly described. In Section 3 the models are compared with the lines detected towards a clump in the CB3 outflow. The results are presented in Section 4 and discussed in Section 5.

2 THE CHEMICAL AND RADIATIVE TRANSFER MODELS

A flow diagram of the method used to compare the observed data with the theoretical models is shown in Fig. 1. A first order estimate of the general physical conditions of the clump, such as the size, the density and the temperature, is derived from the observations and used to describe the physics of the phenomenon in the chemical model. The chemical model predicts the fractional abundances; these are given as input to the radiative transfer model together with the density, the temperature and the beam of the telescope to produce the line profiles that are *directly* compared with the observed profiles. Recently, the same method has been used for modelling the envelope of low mass protostars (Jørgesen et al. 2004; 2005; Schöier et al. 2002; Doty et al. 2004) and it was found to be a powerful tool to probe the physical and chemical structure of the protostellar envelopes as well as the age of the protostar.

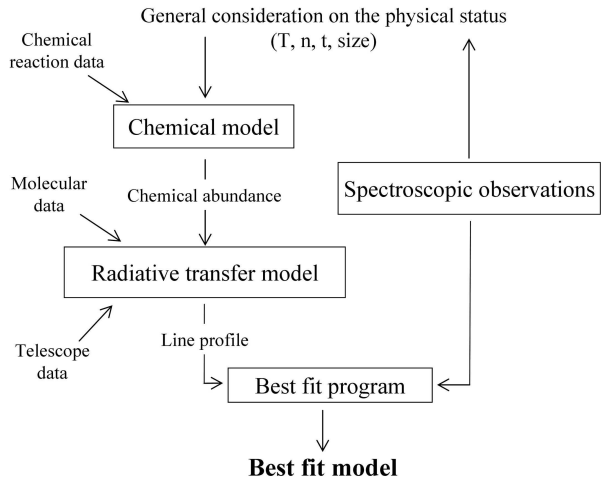


Figure 1. A flow diagram of the scheme applied to compare the observed data to the theoretical models in order to derive the best fit model.

The time-dependent chemical model is described in detail in Paper I. Here we summarize the important characteristics: the chemical network is taken from the UMIST database and includes 221 species involved in 3194 gas-phase and grain reactions. The model is a two-phase calculation. Phase I simulates the formation of a pre-existing clump, or of the homogeneous dark cloud, depending on what scenario we are modelling, and includes freeze-out of the gas on to the grains (see Paper I and below). Phase II simulates the advent of the outflow by warming the clump to 100-200 K or, in the presence of a non-dissociative shock, by increasing the gas temperature to 1000 K for 100 yr and then cooling it down to 100-200 K. As a reminder, the four scenarios considered here (as in Paper I) are:

- Grid A: a pre-existent clump at uniform density warmed by the outflow. In this paper we introduce new models, called As, where the clump at uniform single density is shocked by the outflow;
- Grid B: a pre-existing clump with a density structure shocked by the outflow;
- Grid C: a pre-existing clump with a density structure warmed by the outflow;
- Grid D: a clump formed and warmed or shocked by the outflow.

For each grid different conditions are investigated, changing the model parameters: the depletion efficiency, the type of collapse (free fall or retarded), the grain mantle evaporation (instantaneous or time-dependent), the final density and temperature, the initial sulphur abundance (see Section 4.1), the fraction of frozen H_2CO and CO converted into CH_3OH (see Section 4.4), for a total of 33 models. Each model is time-dependent and evolves for 10^5 yr. See Paper I for a full description of the model and its assumptions, as well as of each scenario.

The chemical abundances produced by the chemical model together with the density and temperature profile are used as input for the radiative transfer model SMMOL (Rawlings & Yates 2001), an approximate Λ -iteration (ALI) code that solves multi-level non-LTE radiative transfer prob-

Table 1. List of the molecules and transitions observed in the S1 clump of the CB3 outflow that are modeled with the radiative transfer code.

specie	line	ν (GHz)
CO	2-1	230.538
CS	3-2	146.967
SO	6 ₅ – 5 ₄	219.949
SO	4 ₃ – 3 ₂	138.178
SO ₂	3 ₁₃ -2 ₀₂	104.029
H ₂ CO	3 ₂₁ -2 ₂₀	218.760
CH ₃ OH	5 ₀ -4 ₀ A ⁺	241.791
CH ₃ OH	5 ₋₁ -4 ₋₁ E	241.767
CH ₃ OH	5 ₀ -4 ₀ E	241.700
CH ₃ OH	3 ₀ -2 ₀ A ⁺	145.103
CH ₃ OH	3 ₋₁ -2 ₋₁ E	145.097
CH ₃ OH	3 ₀ -2 ₀ E	145.094
CH ₃ OH	2 ₀ -1 ₀ A ⁺	96.741
CH ₃ OH	2 ₋₁ -1 ₋₁ E	96.739

lems. The molecular data needed for the calculation are taken from the LAMBDA¹ public database (Schöier et al. 2005), except the CH₃OH-A data which we obtained from D. Flower (private communication). As first step the code calculates the total radiation field and the level populations assuming LTE and the interstellar radiation field as input continuum (Black 1994). It then re-calculates the total radiation field, checks for convergence and repeats the process until convergence is achieved. At each radial point the code generates the level populations and the radiation field. The emergent intensity distributions are then convolved with the telescope beam, so that the model directly predicts the line profiles for a given source as observed with a given telescope (e.g. the IRAM 30-m telescope in this work). The radiative transfer model has been successfully benchmarked with other radiative transfer codes (van Zadelhoff et al. 2002). For each model the radiative transfer program has been run for a selected subset of the time steps of the chemical model for a total of 19 time steps starting from 10³ yr after the formation of the clump to 10⁵ yr.

3 MODELLING THE CLUMPS ALONG CB3

CB3 is a Bok globule at a distance of 2500 pc associated with star formation. In particular, it hosts an intermediate-mass YSO driving a 4 M_⊙ outflow with a mechanical luminosity of 5.6 L_⊙. The outflow has been mapped with the IRAM 30-m telescope in a number of species (Codella & Bachiller 1999) and four molecular clumps were identified along the main axis. The physical conditions derived in the four clumps by Codella & Bachiller (1999) by means of LVG or LTE calculations are very similar to each other, and we use these values to guide the choice of the input parameters in our chemical models. We choose to fit the clump S1 of the CB3 outflow located in the southern lobe at an offset (0'', -30'') from the millimeter driving source since it is the best defined clump. In Table 1 we list all the species and the lines observed in the S1 position for which the molecular data (Einstein coefficients and collisional rates) exist and

the radiative transfer code has been run. Most of these lines have a Gaussian profile with similar width. We adopt a microturbulent velocity of 5 km s⁻¹ for our radiative transfer modelling. This is equivalent to modelling the observed line profiles with a single gaussian line with a fixed FWHM of 10 km s⁻¹. We assume a clump size of 0.12 pc as derived from the IRAM maps. However, we note that most of the emission from the clump is unresolved by the large IRAM-30m beam (HPBW = 10''–29''), so 0.12 pc is most likely an overestimate of the real size of the clump. In Table 2 we list the chemical models computed and their parameters: the name of the model (column 1); the presence (Y) or absence (N) of non-dissociative shock (column 2); the density of the clump (column 3), for models with a density profile we give the two extremes of the range; the final temperature (column 4); the percentage of gas depleted into grains at the end of the Phase I (column 5); the initial sulfur abundance (column 6); and any other relevant parameters that were varied (column 7) such as the type of collapse simulated in Phase I (free-fall or retarded), the percentage of CO or H₂CO converted into CH₃OH on the grain surfaces or the type of evaporation from the grains once the outflow approaches the clumps (instantaneous or time-dependent as in Viti & Williams (1999)). For the models of Grid D we also give the velocity of the outflow. For this work, we extend the grids of models already published in Paper I. In particular, we computed new models for: clumps at uniform density that are shocked (Grid As); clumps with a density profile from 5 × 10⁵ cm⁻³ to 10⁶ cm⁻³ at a temperature of T=200 K; clumps with a density profile from 2.5 × 10⁵ cm⁻³ to 5 × 10⁵ cm⁻³ and from 3 × 10⁵ cm⁻³ to 6 × 10⁵ cm⁻³. From Paper I, we found that most of the models from Grid D, where the clumps are formed by the compression of the incoming outflow, give unphysical results and thus in this paper we restrict our analysis to models D1, D3, D4, D4-shock and D8 only.

To fit the lines listed in Table 1 we used a χ^2 method that simultaneously fits the total integrated flux of the observed transitions of various species. The formula used is:

$$\chi^2 = \frac{1}{N} \sum_{i=1}^N \left[\frac{Flux_{mod}(i) - Flux_{obs}(i)}{Flux_{obs}(i)} \right]^2 \quad (1)$$

where i is the index indicating the line, N is the total number of lines considered, $Flux_{mod}$ is the integrated flux of the model and $Flux_{obs}$ is the observed integrated flux. The difference between the theoretical and observed flux is weighted with the observed flux instead of the error of the measurement because the uncertainties associated to the chemical models are higher than the error of the observations, making it meaningless to use the error as the weight. Moreover, in this way we avoid giving the brighter lines a higher weight. A similar formula has also been used by other authors, e.g. Doty et al. (2004).

4 RESULTS

In the next 5 subsections, we will analyse the results we obtain for the fit of each molecular species separately; in Section 5 we will attempt to fit all the species simultaneously. In order to take into account the uncertainties in the parameters adopted in the models and the calibration errors

¹ <http://www.strw.leidenuniv.nl/~moldata>

Table 2. List of the models and their parameters: presence (Y) or absence(N) of non-dissociative shock, density, final temperature, percentage of freeze-out, initial sulfur abundance and other possible parameters that are different with respect to the other models. For Grid D models the density and temperature are the final ones (at $t=10^5$ yr).

model	shock	$n(\text{H}_2)$ (10^5 cm^{-3})	T (K)	FR (%)	X(S) (10^{-7})	Note
A1	N	1	210	15	130	
A2	N	1	210	35	130	retarded collapse
A3	N	1	210	11	130	retarded collapse
A4	N	1	210	20	19	
A5	N	10	210	20	130	
A6	N	10	210	30	1.3	
A7	N	10	210	55	1.3	
A8	N	10	210	80	1.3	
A9	N	50	210	25	130	
A10	N	5	210	30	1.3	
As1	Y	5	210	30	1.3	
As2	Y	1	210	30	1.3	
B1	Y	5-10	110	40	1.3	
B2	Y	5-10	110	60	1.3	
B3	Y	5-10	110	60	1.3	100% $\text{H}_2\text{CO}\Rightarrow\text{CH}_3\text{OH}$
B4	Y	5-10	110	80	1.3	100% $\text{H}_2\text{CO}\Rightarrow\text{CH}_3\text{OH}$
B5	Y	5-10	110	60	1.3	10% $\text{CO}\Rightarrow\text{CH}_3\text{OH}$
B6	Y	5-10	110	60	1.3	20% $\text{CO}\Rightarrow\text{CH}_3\text{OH}$
B7	Y	5-10	210	60	1.3	
B8	Y	2.5-5	210	40	1.3	
B9	Y	3-6	210	60	1.3	
B10	Y	5-10	210	20	1.3	
B11	Y	3-6	210	40	1.3	
B12	Y	2.5-5	210	60	1.3	
C1	N	5-10	110	40	1.3	
C2	N	5-10	110	60	1.3	
C3	N	5-10	110	60	1.3	100% $\text{H}_2\text{CO}\Rightarrow\text{CH}_3\text{OH}$, time-dependent evaporation
C4	N	5-10	210	60	1.3	
D1	N	5-10	110	20	1.3	$v_{outflow} = 2 \text{ km s}^{-1}$
D3	N	5-10	110	20	1.3	$v_{outflow} = 100 \text{ km s}^{-1}$
D4	N	2.5-5	100	20	1.3	$v_{outflow} = 2 \text{ km s}^{-1}$
D4-shock	Y	5-10	100	20	1.3	$v_{outflow} = 2 \text{ km s}^{-1}$
D8	N	5-10	100	20	1.3	$v_{outflow} = 20 \text{ km s}^{-1}$

of the observations, we assume that we obtain a good match to the models when the theoretical line flux differs less than 10% from the observed flux.

4.1 SO

As already noted in Paper I, if in the chemical model we assume a standard solar initial abundance of sulfur (1.3×10^{-5}) the final abundance of SO is much higher than the observed one. Moreover the radiative transfer model produces strong self-absorption in the lines, which is not present in the observed line profile. The observed SO lines can be better reproduced assuming a depleted sulfur initial abundance of 1.3×10^{-7} as also indicated by previous studies (Viti et al. 2003; Ruffle et al. 1999).

We have detected two lines of SO and, due to the different excitation temperature of these lines (24 and 11 K), their ratio should allow us to constrain the temperature of the gas. Indeed, we see that models with temperature of $T \sim 200$ K are the only models that can reproduce the observed line ratio. In Table 3 we list all the models where both the two SO line fluxes differ $\leq 10\%$ from the observed fluxes,

ordered by increasing χ^2 . The SO column density in all the models ranges from $3.6 \times 10^{14} \text{ cm}^{-2}$ to $6.4 \times 10^{14} \text{ cm}^{-2}$. The models from Grid B are the best ones, while models without a non-dissociative shock and models with low density ($n(\text{H}_2) < 3 \times 10^5 \text{ cm}^{-3}$) do not seem to fit the SO lines at all. In Table 3 we note that models with equal input parameters but two different percentage of freeze-out (B10 and B7 or B9 and B11) can both fit the observed lines but at different epoch. In particular, the models with the lower percentage of freeze-out fit the lines at an early epoch with respect to the models with higher freeze-out. The best fit is given by the model B10 ($n(\text{H}_2) = (5-10) \times 10^5 \text{ cm}^{-3}$, $T \sim 200$ K, $\text{FR} = 20\%$, $\text{Shock} = \text{Y}$) at a time $t = 10^3$ yr with $N(\text{SO}) \sim 4 \times 10^{14} \text{ cm}^{-2}$. However, in the B10 model the SO column density increases with time, it has a maximum at $t = 3 \times 10^4$ yr and then it decreases again to a value similar to the one assumed at $t = 10^3$ yr. This implies that a good fit can also be obtained at a later time of $t = 9 \times 10^4$ yr. The comparison between the observed lines and the best fit model is shown in Fig. 2.

Table 3. List of the best models for the two SO transitions, ordered by increasing χ^2 , with the relative epoch, gas density, temperature, freeze-out and SO column density.

model	epoch (yr)	$n(\text{H}_2)$ (10^5 cm^{-3})	T (K)	FR %	N(SO) (cm^{-2})
B10	1×10^3	5–10	210	20	3.8×10^{14}
A10	5×10^3	5	210	30	6.4×10^{14}
B11	2×10^3	3–6	210	40	5.5×10^{14}
B9	3×10^4	3–6	210	60	5.3×10^{14}
B10	9×10^4	5–10	210	20	3.8×10^{14}
B7	8×10^4	5–10	210	60	3.6×10^{14}

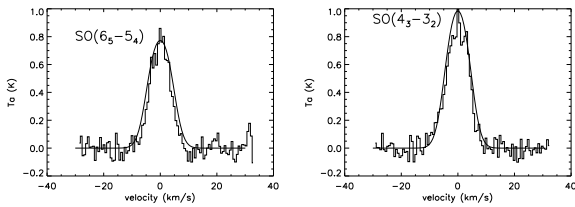


Figure 2. The two SO $6_5 - 5_4$ and $4_3 - 3_2$ lines observed in the clump S1 of the CB3 outflow (histogram) with the line profiles predicted by the best fit model B10 at $t=1 \times 10^3$ yr (continuum line).

4.2 CS

CS is a high density tracer and we find that at a fixed density it is also quite sensitive to the percentage of freeze-out, and in fact models with the same temperature and density but different freeze-out fit the line at different epochs. In 14 out of 33 models, at least a time can be found in which the flux of the CS(3-2) line differs less than 10% from the observed flux (see Table 4) and for 3 models, namely As1, C3 and B9, we find a range of times fitting the line. The models cover almost all the explored parameter space indicating that the CS(3-2) line alone can not be used to constrain the physical conditions of the clump, nor can it be used to discriminate among different scenarios of formation. Despite the different physical parameters, all the models in Table 4 have a similar CS column density: $N(\text{CS}) \sim 10^{14} \text{ cm}^{-2}$. It is worth noting that the best fit model is the model As1 ($n=5 \times 10^5 \text{ cm}^{-3}$, $T \sim 200 \text{ K}$, $\text{FR}=30\%$, $\text{Shock}=Y$) at a time $t=2 \times 10^3$ yr with $N(\text{CS})=1.2 \times 10^{14} \text{ cm}^{-2}$. The comparison between the observed line and the best fit model is shown in Fig. 3. The fact that the modelled line has a peak higher than the observed one suggests that either the line has a FWHM slightly lower than the fixed value of 10 km s^{-1} or the line is weakly self-absorbed.

4.3 SO₂

In Table 5 we report all the models where the SO₂ line flux differs $\leq 10\%$ from the observed flux, ordered, as usual, by increasing χ^2 . The SO₂ column density ranges from 2×10^{14} to $5 \times 10^{14} \text{ cm}^{-2}$. We find that $N(\text{SO}_2)$ is very sensitive to time and in all the models it increases by more than two orders of magnitude from $t=10^3$ yr to $t=10^5$ yr. However,

Table 4. List of the best models for the CS(3-2) transition, ordered by increasing χ^2 , with the relative epoch, gas density, temperature, freeze-out and CS column density.

model	epoch (yr)	$n(\text{H}_2)$ (10^5 cm^{-3})	T (K)	FR %	N(CS) (cm^{-2})
As1	2×10^3	5	210	30	1.2×10^{14}
C1	1×10^5	5–10	110	40	1.2×10^{14}
A4	1×10^3	1	170	20	1.5×10^{14}
A2	3×10^3	1	210	35	1.3×10^{14}
B12	4×10^4	2.5–5	210	60	1.4×10^{14}
B10	5×10^3	5–10	210	20	1.6×10^{14}
D4	2×10^3	10	70	20	2.2×10^{14}
As1	1×10^3	5	210	30	1.1×10^{14}
C3	6×10^3	5–10	110	60	1.1×10^{14}
D8	2×10^3	10	70	20	1.6×10^{14}
B9	4×10^4	3–6	210	60	1.6×10^{14}
C3	5×10^3	5–10	110	60	1.2×10^{14}
B4	3×10^3	5–10	110	80	1.0×10^{14}
C2	4×10^4	5–10	110	60	1.0×10^{14}
B9	3×10^4	3–6	210	60	1.3×10^{14}
As1	3×10^3	5	210	30	1.3×10^{14}
C3	5×10^3	5–10	110	60	1.7×10^{14}
B8	1×10^4	2.5–5	210	40	1.0×10^{14}
As2	1×10^5	1	210	30	1.2×10^{14}

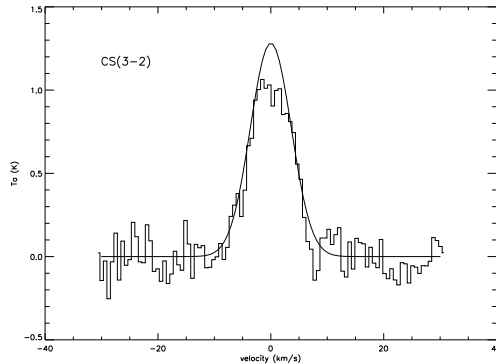


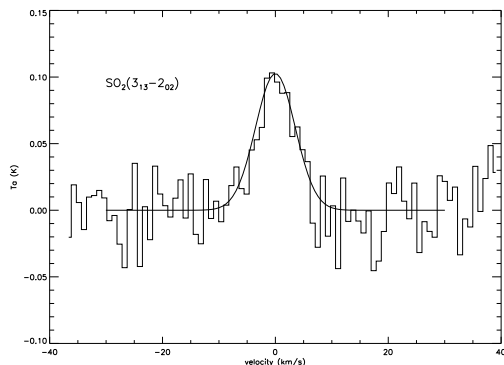
Figure 3. The CS(3-2) line observed in the clump S1 of the CB3 outflow (histogram) and the line profile predicted by the best fit model As1 at $t=2 \times 10^3$ yr (continuum line).

we do not seem to find a good fit for times $> 10^4$ yr. At later times the modeled column density is usually higher than the observed one. Similar to our SO fits, the models from grid B, As and A with high H₂ density ($n \geq 10^6 \text{ cm}^{-3}$) give the best fits, indicating once again that the scenario where the clump is (at least partially) pre-existing the outflow is the most likely. All models from Grid D, C and A (with the exception of A8 and A9 - see below) produce a SO₂ line intensity very different from the observed one, up to two orders of magnitude for the model D4. One common characteristic of these models is the lack of a post-shock phase at high temperature, hence it seems that this species is indeed a good tracer of the presence of a non-dissociative shock. This is in agreement with theoretical models of C-type shocks (Pineau des Forêts et al. 1993) where the abundance of SO₂ is seen to increase after the passage of the shock and SO₂ is the dominant form of sulfur in the post-shock region.

The best fit model (see Fig. 4) is the model A9

Table 5. List of the best models for the SO₂ 3₁₃-2₀₂ transition, ordered by increasing χ^2 , with the relative epoch, gas density, temperature, freeze-out and SO₂ column density.

model	epoch (yr)	n(H ₂) (10 ⁵ cm ⁻³)	T (K)	FR %	N(SO ₂) (cm ⁻²)
A9	6×10 ³	50	210	25	2.5×10 ¹⁴
B1	3×10 ³	5–10	110	40	3.5×10 ¹⁴
A8	2×10 ³	10	210	80	2.6×10 ¹⁴
B8	5×10 ³	2.5–5	210	40	2.7×10 ¹⁴
A8	3×10 ³	10	210	80	2.7×10 ¹⁴
B7	6×10 ³	5–10	210	60	5.1×10 ¹⁴
As1	9×10 ³	5	210	30	2.1×10 ¹⁴
B9	6×10 ³	3–6	210	60	3.3×10 ¹⁴
B3	1×10 ³	5–10	110	60	3.8×10 ¹⁴
A8	4×10 ³	10	210	80	2.8×10 ¹⁴
B11	7×10 ³	3–6	210	40	3.5×10 ¹⁴

**Figure 4.** The SO₂ 3₁₃-2₀₂ line observed in the clump S1 of the CB3 outflow (histogram) with the line profiles predicted by the best fit model A9 at $t=6\times 10^3$ yr (continuum line).

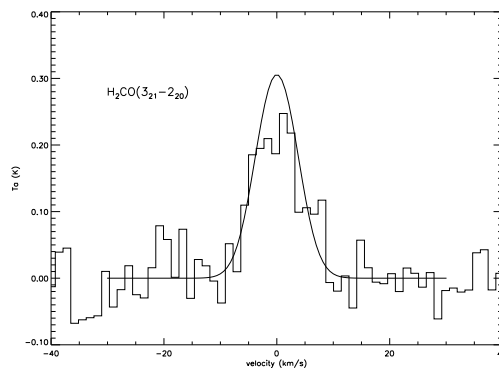
($n=5\times 10^6$ cm⁻³, $T\sim 200$ K, $FR=25\%$, $Shock=N$) at the epoch of $t=6\times 10^3$ yr. We do not think, however, that this model is correct because such high uniform density for a clump of 0.12 pc would imply a visual extinction of more than 1000 mags. Moreover, the initial sulfur abundance for A9 is solar. Probably, in the A9 model the absence of the non-dissociative shock is compensated by the higher initial sulfur abundance and the high density that lead to a SO₂ column density able to fit the line. As can be seen from Table 5 there are quite a number of models that can fit the SO₂ line. It is clear therefore that we can not use this line to deduce uniquely the physical characteristics of our clump. However, the SO₂ line does seem to trace a gas with a density between 3×10^5 and 10^6 cm⁻³ and a temperature between 100 and 200 K. The freeze-out parameter is not constrained at all since in the models that fit the data the freeze-out parameter ranges from 25% to 80%. This is not surprising since SO₂ is a second generation species which forms after the dissociation of other sulfur bearing species released from the grains.

4.4 H₂CO

In Table 6 we report all the models that fit the observed flux of the H₂CO 3₂₁-2₂₀ line within 10%. Good fits can

Table 6. List of the best models for the H₂CO 3₂₁-2₂₀ transition, ordered by increasing χ^2 , with the relative epoch, gas density, temperature, freeze-out and H₂CO column density.

model	epoch (yr)	n(H ₂) (10 ⁵ cm ⁻³)	T (K)	FR %	N(H ₂ CO) (cm ⁻²)
As1	1×10 ³	5	210	30	6.1×10 ¹⁴
B3	1×10 ³	5–10	110	60	6.5×10 ¹⁴
B11	4×10 ³	3–6	210	40	6.5×10 ¹⁴
B10	4×10 ³	5–10	210	20	5.1×10 ¹⁴
As1	2×10 ³	5	210	30	6.6×10 ¹⁴
B8	3×10 ³	2.5–5	210	40	6.0×10 ¹⁴
B10	3×10 ³	5–10	210	20	4.5×10 ¹⁴

**Figure 5.** The H₂CO 3₂₁-2₂₀ line observed in the clump S1 of the CB3 outflow (histogram) with the line profiles predicted by the best fit model As1 at $t=1\times 10^3$ yr (continuum line).

be obtained in models with non-dissociative shocks (Grid B and As). In the models without them (Grid A, C and D) the formaldehyde is usually overabundant. This is because it is mainly formed by the reaction of oxygen with CH₃. In models with a non-dissociative shock, during the high temperature phase, the oxygen mainly interacts with neutrals to form OH and H₂O, thus there is less oxygen free to form H₂CO. H₂CO is one of the species most sensitive to time; indeed its abundance increases by more than one order of magnitude from $t=10^3$ yr to $t=10^5$ yr. A good fit can only be found for very early epochs of $\leq 4\times 10^3$ yr. As in Paper I we find that if the clumps evolve for more than 5×10^3 yr after the high temperature phase, the theoretical abundance of H₂CO is always overabundant with respect to the observations. Even in models where we allow conversion of H₂CO to methanol on the grains (B3 and B4) an acceptable fit can only be obtained at $t=10^3$ yr for the B3 model. The H₂CO column density in the selected models ranges from 4.5×10^{14} to 6.5×10^{14} cm⁻² and the freeze-out parameter ranges between 20% and 60% while the temperature is ~ 200 K, with the exception of the B3 model. The best fit model is As1 ($n(H_2)=5\times 10^5$, $T\sim 200$ K, $FR=30\%$, $Shock=Y$) at the time $t=10^3$ yr and column density $N(H_2CO)=6.1\times 10^{14}$ cm⁻². In Fig. 5 the As1 model is plotted superimposed to the observed line spectrum.

4.5 CH₃OH

Methanol has always been considered a good tracer of the physical condition of the emitting gas (e.g. Kalenskii et al. 1997, Leurini et al. 2004). In particular, it has been used as probe of density in high-density medium (e.g. Menten et al. 1988) and a temperature estimate can be easily derived from the rotational diagram, if multiple transitions are available. Moreover, the presence of several transitions close in wavelength make it easy to observe more lines simultaneously, increasing the number of observational constraints and minimizing the relative calibration uncertainties.

The Boltzmann plot of the 8 methanol lines observed in the S1 clump gives a column density $N(\text{CH}_3\text{OH}) \sim 10^{16} \text{ cm}^{-2}$ and a rotational temperature of only 16 K (Codella & Bachiller 1999), well below the 200 K we derived from the other molecules. However, in the physical conditions typical of outflows the gas is not in LTE condition and it is subthermally excited so that the rotational temperature estimated from the Boltzmann plot is below the kinetic temperature (Bachiller et al. 1995).

In the radiative transfer model the A and E types of methanol must be considered as separate species since the transition between the two symmetry states can not happen at a significant rate by radiative or collisional processes. We assume the standard ratio of 1 between A and E methanol as also suggested by the absence of a significant shift in the A and E transitions in the Boltzmann plot. This choice has also been verified a posteriori since we find that both A and E methanol lines have similar deviation with respect to the observed lines.

From Table 1 we see that the 3_K-2_K and 2_K-1_K transitions are very close in frequency. The line rest frequencies of the CH₃OH 3₀-2₀ A⁺ (145.103 GHz) and 3₋₁-2₋₁ E (145.097 GHz) transitions are separated by 12.4 km s⁻¹, those of the 3₋₁-2₋₁ E (145.097 GHz) and 3₀-2₀ E (145.094 GHz) by 6.2 km s⁻¹. The 2₀-1₀A⁺ (96.741 GHz) and 2₋₁-1₋₁ E (96.739 GHz) transitions are also separated by 6.2 km s⁻¹. Since the separation of the lines is similar or lower than the typical FWHM in the clump (10 km s⁻¹) we expect that 3_K-2_K and 2_K-1_K transitions overlap with each other. Indeed the lines at 145.1 and 96.7 GHz are blended; thus photons at these frequencies will see a higher optical depth than expected, because they are “seeing” the line profiles of neighbouring transitions. The SMMOL code does not yet have a line-overlap facility, so our modelling of these blended methanol transitions is semi-quantitative. For this reason we consider as an acceptable fit for the methanol all the models that produce line fluxes that differ less than 30% with respect to the observed flux, instead of 10% as used for the other species.

None of our models are able simultaneously to fit all of the 8 methanol transitions (5 lines of CH₃OH-E and 3 lines of CH₃OH-A). In particular, we find that in models where the higher energy transitions (5_K-4_K) are reproduced, the lower energy transitions (3_K-2_K and 2_K-1_K) are largely underestimated. Conversely, models that reproduce the lower energy transitions overestimate the transitions at higher energy. This could be a direct consequence of the effects of line-overlap in the 3_K-2_K and 2_K-1_K transitions: the low energy transitions are simply “seeing” more optical depth than the higher energy transitions.

Table 7. List of the best models for the 3 lines of the CH₃OH 5_K-4_K transition (both A and E type), ordered by increasing χ^2 , with the relative epoch, gas density, temperature, freeze-out and methanol column density. The last 2 models have a smaller clump size of 0.05 pc

model	epoch (yr)	n(H ₂) (10 ⁵ cm ⁻³)	T (K)	FR %	N(CH ₃ OH) (cm ⁻²)
D1	(9-10)×10 ⁴	5-10	110	20	(4.2-4.8)×10 ¹⁴
B12	(8-9)×10 ³	2.5-5	210	60	(4.3-4.7)×10 ¹⁴
D8	1×10 ⁵	5-10	100	20	5.2×10 ¹⁴
D4	7×10 ⁴	3-5	100	20	4.3×10 ¹⁴
A10	(1-10)×10 ⁴	5	210	30	(1.2-1.5)×10 ¹⁵
As1	(1-4)×10 ³	5	210	30	1.5×10 ¹⁵

We did test, however, whether these inconsistencies are due to incorrectness of our basic assumptions on the physical condition of the clump; we computed further models where we assumed: *i*) a lower temperature of T=20 K or *ii*) a smaller size of the clump of 0.06 pc. Again, there is no single model able to fit both the lower and the higher energy transitions at the same time. Another possible explanation is that the high energy transitions trace a different component of the gas, possibly with different physical (and chemical) characteristics. Indeed the 5_K-4_K lines seem to be fitted with models that produce a methanol column density $N(\text{CH}_3\text{OH}) \sim 5 \times 10^{14} \text{ cm}^{-2}$ while the 3_K-2_K and 2_K-1_K lines are fitted by models that have a higher column density $N(\text{CH}_3\text{OH}) \sim 5 \times 10^{15} \text{ cm}^{-2}$. Hence, we tried to separately fit the two components. For the high energy transitions (the 5_K-4_K lines) we find that most of the models that fit the lines belong to Grid D (see Table 7), indicating that these transitions may trace a gas compressed by the outflow (scenario D). Note that the models in Grid D have a lower abundance of methanol than the models in the other grids. This is due to reduced amount of frozen material, since methanol is preferentially formed on the grains via hydrogenation of a fraction of CO and H₂CO: in the scenario depicted in Grid D the clump is formed by the compression of the outflow, and therefore the timescale available for freeze out is quite short, as explained in detail in Paper I. Moreover during the clump formation the temperature also increases, slowing significantly the freeze out. While it is possible that the high *J* transitions trace a newly formed clump (scenario of Grid D), it is also possible that this lower column density component simply traces a smaller component of the clump. To test this hypothesis we recomputed models A10 and As1 assuming a smaller clump size of 0.04, 0.05 and 0.06 pc instead of 0.12 pc. We found that both models A10 and As1 were able to fit the 3 CH₃OH lines of the 5_K-4_K transition within 30% with a clump size of 0.05 pc (see Table 7).

As discussed above the three 3_K-2_K lines and the two 2_K-1_K lines are closely blended due to line-overlap effects. Therefore to attempt a fit to the 5 CH₃OH lines of the 3_K-2_K and 2_K-1_K transitions, we decided to calculate the χ^2 considering the sum of the flux of all the blended lines rather than each line flux separately. We find that two of our models fit the 5 lines (see Table 8). The best fit model is B10 ($n(\text{H}_2) = (5-10) \times 10^5 \text{ cm}^{-3}$, T~200 K, FR=20%, Shock = Y) with a column density $N(\text{CH}_3\text{OH}) = 7 \times 10^{15} \text{ cm}^{-2}$. The best

Table 8. List of the best models for the 5 lines of the CH₃OH 3_K-2_K and 2_K-1_K transitions (both A and E type), ordered by increasing χ^2 , with the relative epoch, gas density, temperature, freeze-out and methanol column density.

model	epoch (yr)	n(H ₂) (10 ⁵ cm ⁻³)	T (K)	FR %	N(CH ₃ OH) (cm ⁻²)
B10	6×10 ⁴	5–10	210	20	7×10 ¹⁵
C3	7×10 ⁴	5–10	110	60	3×10 ¹⁵

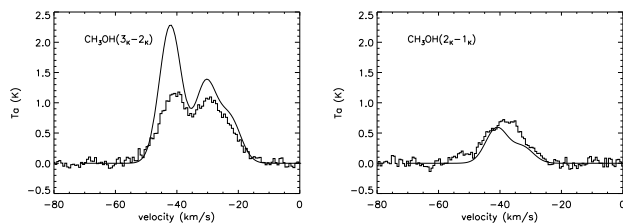


Figure 6. The CH₃OH 3_K-2_K and 2_K-1_K lines observed in the clump S1 of the CB3 outflow (histogram) and the line profile predicted by the best fit model B10 at $t=6\times 10^4$ yr (continuum line).

fit time is $t=6\times 10^4$ yr, although in B10 the methanol column density is quite constant in time so it is not possible to constrain the age of this component. In Fig. 6 we show the best fit model: although the total flux of the three blended 3_K-2_K lines are still within the 30% of tolerance, we do not achieve a good fit for the CH₃OH 3₀-2₀ A⁺ line at -41.5 km s⁻¹. We note that in all the models the ratio between the 3₀-2₀ A⁺ and the 3₀-2₀ E lines is always higher (up to a factor of 1.5) than the observed value indicating a systematic trend to overestimate the 3₀-2₀ A⁺ irrespective of the model parameters. This is due to the effect of line overlap that is not included in our radiative transfer model.

Despite the limitation due to the lack of line-overlap effect in the modeling, our analysis seems to indicate the presence of two different methanol components: one with lower column density $N(\text{CH}_3\text{OH}) \sim 5\times 10^{14}$ - 10^{15} cm⁻², and possibly with smaller size, traced by the higher energy transitions, and another with higher column density $N(\text{CH}_3\text{OH}) \sim 7\times 10^{15}$ cm⁻² and probably at lower excitation conditions since it is traced by the lower energy lines. In our analysis we assumed the same temperature for both components; this may be unrealistic but we believe that in any case neither of the two components has a temperature less than 100 K, due to the presence of the outflow. The possibility of different components or substructures within the clump was already put forward in Paper I for CB3 and partly confirmed by the better fits obtained for L1157 where the substructure is in fact observationally resolved.

5 DISCUSSION

In the previous section we have shown that, if one considers each species separately, it is indeed possible to find a very good fit for each species. The column densities we

find are always within a factor of 3 of the ones derived by Codella & Bachiller (1999) by using LTE or LVG models.

We now attempt to find a model that simultaneously fits *all* the molecular transitions observed in the S1 clump. In order to take into account the large uncertainties in the model for the global fit we consider acceptable all the models where the line flux differs less than 50% from the observed flux. We choose this relatively high level of tolerance because the line emission depends, directly or indirectly, on many parameters that are not well known such as the size of the emitting region, the density, the temperature and the chemical abundances that in turn depend on other parameters such as the percentage of depletion of the gas on to the grains, the efficiency of some reactions, the density structure etc, and each species/transition has a different sensitivity to each parameter. We find that none of the 33 models is able to fit simultaneously all the molecular lines within 50% indicating, as also suggested in Paper I, that indeed several gas components exist in the IRAM-30m beam.

In order to identify the different components we consider different groups of molecules. Firstly, we consider all the S-bearing molecules i.e. CS, SO, SO₂. None of the 33 models are able to fit all the 4 observed lines. In particular, while several models fit both the CS and SO transitions (see Table 9) the same models do not fit the SO₂ line that is usually fitted at the earlier times of $t < 10^4$ yr (see Table 5). The best fit model for CS and SO is the model B9 at a time of $t=3\times 10^4$ yr (see Fig. 7); however, at that time, the SO₂(3₁₃-2₀₂) line is 8 times more intense than the observed emission (see Fig. 8 where the column density of the species is plotted versus time). In the same model the SO₂ line can however be fitted at an early time, $t=6\times 10^3$ yr, when the column density is $N(\text{SO}_2)=3\times 10^{14}$ cm⁻². Since in most of the models the SO₂ abundance increases significantly with time, the fact that the SO₂(3₁₃-2₀₂) line is fitted by young epoch (see Table 5) indicates that a low quantity of SO₂ is needed to fit the line. A low column density of SO₂ can be obtained not just with a low chemical abundance but also with a smaller size of the clump. In fact a smaller component in the clump has been already suggested by the analysis of the methanol lines. As we did for the methanol, we test this possibility considering the chemical models A10 and As1 with a smaller clump size of 0.04, 0.05 and 0.06 pc. In the A10 models the SO₂ abundance is always lower than that in the As1 model due to the lack of a high temperature phase in the former model. The A10 model does not succeed in fitting the observed SO₂(3₁₃-2₀₂) line. On the contrary, a very good fit can be obtained if we assume a size of 0.05 pc for the model As1 at the epoch $t=4\times 10^4$ yr. At this epoch, the model As1 also fits the 3 higher energy lines of methanol (see Fig. 9), as already shown in Section 4.5. The same model does not fit the CS and SO lines. We therefore conclude that SO₂ and the higher energy methanol 5_K-4_K lines may be emitted from a smaller gas component with a size of $d\sim 0.05$ pc, $n(\text{H}_2)\sim 5\times 10^5$ cm⁻³ and $T\sim 200$ K. This component is associated with emission at high excitation of molecules produced in high temperature gas thus it could trace the zone of stronger interaction between the outflow and the clump.

Next we attempt to fit simultaneously the CS and SO transitions together with the 5 lower energy transitions of CH₃OH (3_K-2_K and 2_K-1_K). We find no models able to fit

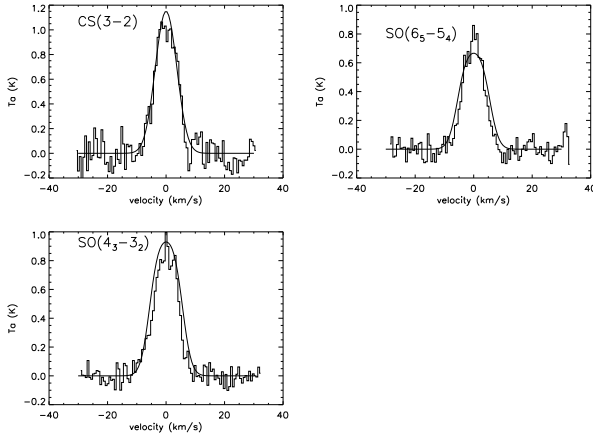


Figure 7. The CS and SO lines observed in the clump S1 of the CB3 outflow (histogram) with the line profile predicted by the best fit model B9 at $t=3 \times 10^4$ yr (continuum line).

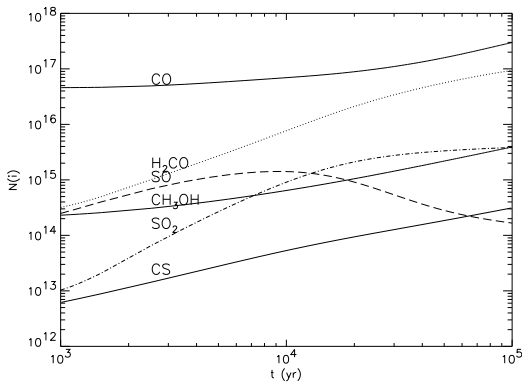


Figure 8. Column densities versus time for the B9 model.

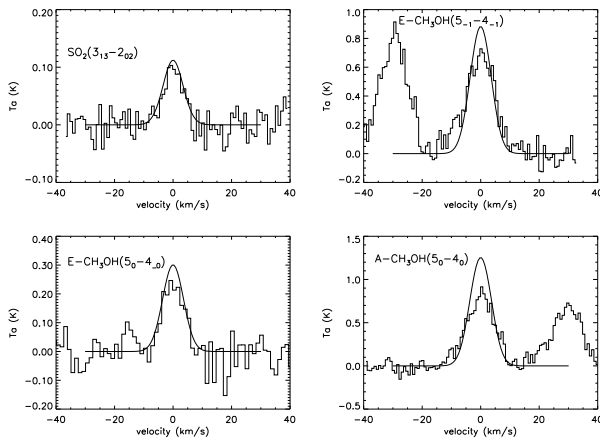


Figure 9. The $\text{SO}_2(3_{13}-2_{02})$ and $\text{CH}_3\text{OH}(5_K-4_K)$ lines observed in the clump S1 of the CB3 outflow (histogram) with the line profile predicted by the best fit model As1 at $t=4 \times 10^4$ yr (continuum line). The size of the clump is $d=0.05$ pc.

Table 9. List of the best models for the $\text{SO}(6_5-5_4)$, $\text{SO}(4_3-3_2)$ and $\text{CS}(3-2)$ lines, ordered by increasing χ^2 , with the relative epoch, χ^2 , gas density temperature and freeze-out.

model	epoch (yr)	$n(\text{H}_2)$ (10^5 cm^{-3})	T (K)	FR %
B9	3×10^4	3–6	210	60
As1	1×10^3	5	210	30
B4	2×10^3	5–10	110	80
B12	2×10^4	2.5–5	210	60
B12	3×10^4	2.5–5	210	60
As1	2×10^3	5	210	30
A1	2×10^3	1	210	15

simultaneously the 3 species within 50%. In fact, from the fitting of the single species (see Section 4.5) we see that the low energy methanol lines seem to trace a slightly higher density (model B10 with $n(\text{H}_2)=(5-10) \times 10^5 \text{ cm}^{-3}$) than the CS and SO component (model B9 with $n(\text{H}_2)=(3-6) \times 10^5 \text{ cm}^{-3}$), but the same temperature ($T \sim 200 \text{ K}$) and very similar time (6×10^4 yr and 3×10^4 yr respectively). However the difference in the density is not so relevant, considering also the high uncertainties in the model especially for methanol because of line overlap effects, and we think that probably the low energy transitions of CH_3OH could be associated with the same extended gas component traced by CS and SO.

Finally we check whether the $\text{H}_2\text{CO} 3_{21}-2_{20}$ line could be associated with one of the two identified components. We find that the B9 model with clump size of 0.12 pc at $t=3 \times 10^4$ yr predicts a line about 25 times brighter than the observed one. Indeed, as said in Section 4.4, assuming a size of 0.12 pc the H_2CO can be fitted only at very early epoch ($t \leq 4 \times 10^3$ yr) while for more evolved times all the models predict far too much H_2CO . On the other hand, if we consider the smaller component, i.e. the As1 model at 4×10^4 yr with clump size of 0.05 pc, the theoretical intensity is only 3 times higher than the observed one, while at the early epoch of 2×10^4 a very good fit (within 20%) of the observed line is obtained. Although a global fit of the H_2CO with the SO_2 and high J CH_3OH lines cannot be obtained within the 50% of tolerance, we think that H_2CO does not trace the whole clump but is associated with the smaller gas component and it is probably emitted by a region even smaller than 0.05 pc.

The S1 clump has also been observed in the CO (2-1) line; however the profile of this transition is very different with respect to all the other lines: a blue non-Gaussian line wing and a self absorption at the ambient LSR velocity (-38.5 km^{-1}) are present in the line. This profile indicates that the line has a substantial contribution from the large scale outflowing gas and also that part of the emission is self absorbed by the ambient cloud. Moreover, Codella & Bachiller (1999) estimate a temperature of $\sim 10 \text{ K}$ for the CO at all the line velocities and they find that the (2-1) line is optically thick showing that the emission is dominated by the outer, colder part of the outflow rather than by the S1 clump. All these considerations lead us to not consider the CO (2-1) line for the global fit of the S1 clump. However, we still ran the radiative transfer code for CO in order to roughly evaluate if in the best fit models the contribution of the clump to

this line is negligible as we expected. Indeed, we find that in the B9 model, that fits CS and SO, the predicted CO(2-1) flux is only 23% of the observed flux.

We find that some species are very sensitive to time, such as S-bearing molecules, in agreement with several previous studies (Hatchell et al. 1998, Viti et al. 2001, Wakelam et al. 2005, Codella et al. 2005), and they can therefore be used to determine the age of the S1 clump. We fit both the components of the clump with the same time $\sim 3\text{--}4 \times 10^4$ yr which is similar to the dynamical time of the S1 clump estimated from the SiO emission ($t \sim 10^5$ yr, Codella & Bachiller 1999). Note however that our starting point ($t=0$) in all scenarios is set to be when the outflow starts interacting with the surrounding environment hence the age we derive is not necessarily the age of the outflow.

6 CONCLUSIONS

A time-dependent chemical model has been coupled with a radiative transfer code to model the observed molecular lines emission in the small chemically rich clump S1 along the south lobe of the CB3 outflow. This proved to be a powerful tool in constraining the physical and chemical parameters of the gas, especially when there is more than one transition of the same molecule.

We find that more than one model is able to fit the line emission of single species. Hence to constrain the physical parameters of our clump a multi-line analysis is needed.

Different scenarios for the formation of the clump have been investigated within a large range of physical conditions. Our results show that most of the observed lines can not be fitted by models from the scenarios A, C and D. On the contrary, the models from scenario B or As seem to reproduce most of our data. This is consistent with our previous findings (see Paper I). We conclude that the observed dense clumps are, at least partially, formed prior to the advent of the outflow. The advent of the outflow on such clumps leads to a short phase of high temperature ($T \sim 1000$ K) followed by fast cooling down to temperatures of ~ 200 K.

In addition to the large scale outflowing gas traced by the non-Gaussian wings detected in the CO (2-1) line, we identify two other components inside the large IRAM-30m beam. The extended component ($d=0.12$ pc) is traced by CS and SO and probably by the lower energy transitions ($3_K\text{--}2_K$ and $2_K\text{--}1_K$) of CH₃OH. This component is not uniform in density but it has a density structure in the range $3 \times 10^5\text{--}10^6$ cm⁻³. The second component is more compact, with size ~ 0.05 pc and density $\sim 5 \times 10^5$ cm⁻³, and it is traced by SO₂, H₂CO and the $5_K\text{--}4_K$ CH₃OH lines. For both the components we estimated a similar temperature ($T \sim 200$ K) and time ($t \sim 3 \times 10^4$ yr) from when the clump has started to interact with the outflow. Since the compact component is traced by the higher energy transitions of CH₃OH, it is probably at higher excitation and may trace the zone of stronger interaction between the outflow and the clump. However, the analysis of the CH₃OH data needs to be confirmed by modelling of the data with a radiative transfer code that takes into account the effects of line-overlap (Gray & Yates, in prep).

ACKNOWLEDGEMENTS

We are grateful to Prof. D.R. Flower for providing us with the molecular data of the CH₃OH-A. SV acknowledges individual financial support from a PPARC Advanced Fellowship. This work was partly carried out on the PSE supercomputer at the HiPerSPACE Computing Centre, UCL, which is funded by the UK Particle Physics and Astronomy Research Council.

REFERENCES

- Bachiller R., Martín-Pintado J., Fuente A., 1991, *A&A*, 243, L121
- Bachiller R., Liechti S., Walmsley C.M., Colomer F., 1995, *A&A*, 295, L51
- Bachiller R., Pérez Gutiérrez M., Kumar M.S.N., Tafalla M., 2001, *A&A*, 372, 899
- Black J.H., 1994, in Cutri R.M., Latter W.B., eds, ASP Conf. Ser. Vol. 58, The first symposium on the infrared cirrus and diffuse interstellar clouds, p. 355
- Codella C., Bachiller R., 1999, *A&A*, 350, 659
- Codella C., Bachiller R., Benedettini M., Caselli P., Viti S., Wakelam V., 2005, *MNRAS*, 361, 244
- Doty S.D., Schöier F.L., van Dishoeck E.F., 2004, *A&A*, 418, 1021
- Deutrey A., Guilloteau S., Bachiller R., 1997, *A&A*, 317, L55
- Hatchell J., Thompson M.A., Millar T.J., Macdonald G.H., 1998, *A&A*, 338, 713
- Jørgesen J.K., Schöier F.L., van Dishoeck E.F., 2004, *A&A*, 416, 603
- Jørgesen J.K., Schöier F.L., van Dishoeck E.F., 2005, *A&A*, 437, 501
- Kalenskii S.V., Dzura A.M., Booth R.S., Winnberg A., Alakoz A.V., 1997, *A&A*, 321, 311
- Leurini S., Schilke P., Menten K.M., Flower D.R., Pottage J.T., Xu L.H., 2004 *A&A*, 422, 573
- Menten K.M., Walmsley C.M., Henkel C., Wilson T.L., 1988, *A&A*, 198, 253
- Pineau des Forêts G., Roueff E., Schilke P., Flower D., 1993, *MNRAS*, 262, 915
- Rawlings J.M.C., Yates J.A., 2001, *MNRAS*, 326, 1423
- Richer J.S., Shepherd D.S., Cabrit S., Bachiller R., Churchwell E., 2000, in Mannings V., Boss A.P., Russell S.S., eds, *Protostars and Planetes IV*, University of Arizona Press, p. 867
- Ruffle D.P., Hartquist T.W., Caselli P., Williams D.A., 1999, *MNRAS*, 306, 691
- Schöier F.L., Jørgesen J.K., van Dishoeck E.F., Blake G.A., 2002, *A&A*, 390, 1001
- Schöier F.L., van der Tak F.F.S., van Dishoeck E.F., Black J.H., 2005, *A&A*, 432, 369
- van Zadelhoff G.J., et al., 2002, *A&A*, 395, 373
- Viti S., & Williams D. A., 1999, *MNRAS*, 310, 517
- Viti S., Caselli P., Hartquist T.W., Williams D. A., 2001, *A&A*, 370, 1017
- Viti S., Girart J. M., Garrod R., Williams D. A., Estalella R., 2003, *A&A*, 399, 187
- Viti S., Codella C., Benedettini M., Bachiller R., 2004, *MNRAS*, 350, 1029 (Paper I)

Wakelam V., Ceccarelli C., Castes A., Lefloch B., Loinard L., Faure A., Schneider N., Benayoun J., 2005, *A&A*, 437, 149